On the nature of metallic nanoparticles obtained from molecular Co_3Ru–carbonyl clusters in mesoporous silica matrices†‡

Fanny Schweyer-Tihay,§[abc] Claude Estournès,¶*[a] Pierre Braunstein,*[b] Jean Guille,[a] Jean-Louis Paillaud,*[c] Mireille Richard-Plouet‖[a] and Jacky Rosé[b]

DOI: 10.1039/b603404g

We report on the impregnation of THF solutions of the low-valent heterometallic cluster $NEt_4[Co_3Ru(CO)_{12}]$ into two mesoporous silica matrices, amorphous xerogels and ordered MCM-41, and a study of its thermal decomposition into metallic nanoparticles by X-ray diffraction, transmission electron microscopy and *in situ* magnetic measurements under controlled atmospheres. The decomposition of the cluster was monitored as a function of temperature by examining the chemical composition of the particles, their size distributions and their structures as well as their magnetic properties. Treatment under inert atmosphere (*i.e.* argon) at temperatures below 200 °C resulted in the formation of segregated spherical particles of *hcp*-ruthenium (2.3 ± 1.0 nm) and *hcp*-cobalt (3.1 ± 0.9 nm). The latter is transformed to *fcc*-cobalt (3.2 ± 1.0 nm) above 270 °C. At higher temperatures, Co–Ru alloying takes place and the Ru content of the particles increases with increasing temperature to reach the nominal composition of the molecular precursor, Co_3Ru. The particles are more evenly distributed in the MCM-41 framework compared to the disordered xerogel and also show a narrower size distribution. Owing to the different magnetic anisotropy of *hcp*- and *fcc*-cobalt, which results in different blocking temperatures, we were able to clearly identify the products formed at the early stages of the thermal decomposition procedure.

Introduction

Nanostructured materials can sometimes show unique physical and chemical properties, different from those of the bulk[1–8], and consequently they have attracted much attention for their magnetic, optical, electrical, and catalytic properties, and their potential applications.[9–15] Several physical or chemical routes have been employed to prepare or synthesize nanoparticles.[15–17] Control over their size,[18–20] shape[21–23] and chemical stability[24–27] is of crucial importance. The reactivity of metallic nanoparticles is considerably enhanced owing to their surface:volume ratios; however, they can be stabilized once precipitated in polymer[25,28,29] or glassy[30–35] matrices. One way to modulate the spatial distribution and chemical stability of nanoparticles is to incorporate them in a host matrix having a meso- or nanoporous architecture. For this purpose, mesoporous materials of very high surface area, such as MCM-41, FSM-16 and SBA-15, have been targeted as host matrices for catalytically-active phases like noble or rare-earth metals,[21–23,36–45] transition metals oxides[46–50] or phosphides.[51–53] Following initial work which demonstrated that low oxidation-state, organo-bimetallic clusters impregnated on a silica support are valuable precursors to bimetallic nanoparticles and that they can display unique catalytic properties,[54–56] we recently extended this methodology to produce metallic nanoparticles by mild, controlled thermal decomposition under inert atmosphere of a heterometallic Co–Ru carbonyl cluster in mesoporous silica xerogel or MCM-41-type matrices.[57] We were, in particular, interested in investigating the influence of an ordered matrix, such as MCM-41, on possible confinement effects that could lead to metal particles with narrower size distribution, and we present here new data on the characterization and physical properties of the resulting metal nanoparticles.

[a] *Groupe des Matériaux Inorganiques, Institut de Physique et Chimie des Matériaux, UMR 7504 CNRS, 23 rue du Loess, 67037 Strasbourg Cedex, France. E-mail: claude.estournes@ipcms.u-strasbg.fr*

[b] *Laboratoire de Chimie de Coordination, UMR 7177 CNRS, Université Louis Pasteur, 4 rue Blaise Pascal, 67070 Strasbourg Cedex, France. E-mail: braunst@chimie.u-strasbg.fr*

[c] *Laboratoire de Matériaux à Porosité Contrôlée, UMR 7016 CNRS, Ecole Nationale Supérieure de Chimie de Mulhouse, 3 rue Alfred Werner, 68093 Mulhouse Cedex, France. E-mail: JL.Paillaud@univ-mulhouse.fr*

§ Present address: Institut Français du Pétrole Lyon, BP 3, 69390 Solaize, France.

¶ Present address: Plate-forme Nationale de Frittage Flash, CIRIMAT, UMR CNRS 5085-Université Paul Sabatier, 118 route de Narbonne, 31062 Toulouse Cedex 04, France.E-mail: estournes@chimie.ups-tlse.fr.

‖ Present address: Institut des Matériaux Jean Rouxel, Laboratoire de Chimie des Solides, 2, rue de la Houssinière, BP 32229, 44322 Nantes Cedex, France.

Experimental

Synthesis of the precursors

Synthesis of ordered mesoporous silica MCM-41[58]. The procedure was slightly modified with respect to the original

one. The molar composition of the mixture is the following: 1 SiO_2 : 0.8 NaOH : 0.2 C_{16}TMABr (hexadecyltrimethyl ammonium bromide) : 135 H_2O. First, CTMABr was introduced into a polyethylene bottle and dissolved in 700 ml of water heated to 35 °C, forming a soap solution. 105 g of sodium silicate, dissolved in 110 ml of water, were added to the soap solution and the mixture was stirred for 10 min. Then, 280 ml of hydrochloric acid (1 M) was added under vigorous stirring to bring the pH of the solution to 12, thus allowing the silica to precipitate around the micelles. After the mixture was stirred for 2 h, the precipitate and the mother liquor were placed in an oven at 100 °C for 24 h. The precipitate was then filtered, washed carefully with distilled water and dried at 40 °C. To eliminate any remaining soap from the pores, the precipitate was placed in a porcelain cup and calcined under air at 600 °C for 4 h before use.

Synthesis of the mesoporous silica xerogels[59]. A sol–gel mixture was prepared from tetramethylorthosilicate (TMOS), methanol, 0.1 M nitric acid aqueous solution and formamide, the molar composition of the mixture being: 1 TMOS : 4 MeOH : 0.45 HNO_3 : 4.5 H_2O : 1 $HCONH_2$. Dilute acid (8.1 g) and formamide (4.5 g) were mixed in a beaker. TMOS (15.22 g) and the alcohol (12.8 g) were added simultaneously to this solution. Further stirring was maintained for 1 h. The sol was then poured into parallelepiped containers and aged in an oven at 40 °C for 5 d. The resulting gels were dried under a flow of argon for 2 d, then under vacuum for 24 h. The monoliths thus obtained were calcined up to 500 °C in order to decompose the organics.

Synthesis of the cluster $NEt_4[Co_3Ru(CO)_{12}]$[60]. The synthesis of the cluster was performed in two steps. The first concerns the preparation of $NEt_4[RuCl_4(CH_3CN)_2]$. A solution of 4.0 g of commercial ruthenium chloride ($RuCl_3$, xH_2O) in 80 ml of HCl (12 N) was heated under reflux at 90 °C for 10 h. This solution was then cooled to room temperature and 3.7 g of $[NEt_4]Cl \cdot xH_2O$ in 40 ml of water and 1 ml of Hg were added. The mixture was stirred for 3 h and the blue–green solution obtained was decanted and filtered in order to eliminate the precipitated mercury salt. The remaining solution was evaporated at 50 °C. The green solid recovered was suspended in 80 ml of CH_3CN and stirred under reflux for 10 h. The resulting yellow solution was mixed with 100 ml of diethylether and placed in a freezer for 2 d. The resulting yellow precipitate of $NEt_4[RuCl_4(CH_3CN)_2]$ was collected, washed with diethylether and dried under vacuum.

In the second stage, 1.50 g of $NEt_4[RuCl_4(CH_3CN)_2]$ in 30 ml of THF were introduced in a Schlenk tube containing a solution of 2.45 g of $Co_2(CO)_8$ in THF. This mixture was heated under reflux for 3 h. The resulting red solution was kept at −40 °C overnight, and $CoCl_2$ precipitated. The solution was filtered, evaporated to dryness and 50 ml of saturated aqueous solution of NEt_4Cl was added in order to dissolve the remaining salt. The red precipitate of $NEt_4[Co_3Ru(CO)_{12}]$ was collected by filtration, dissolved in THF and recrystallized from a THF/hexane mixture at −20 °C.

Characterization techniques

Porosity measurements. Specific surface areas have been determined by nitrogen adsorption/desorption isotherms on a Sorpty 1750 porosimeter. The average diameter of the pores has been estimated by the BET method on a ASAP 2010 Micromeritics apparatus.

X-Ray powder diffraction. A Philips PW-1130 instrument equipped with a copper anticathode ($\lambda_{K\alpha}$ = 1.5418 Å) was used to characterize the undoped matrices while a Siemens D500 diffractometer equipped with a cobalt anticathode ($\lambda_{K\alpha}$ = 1.78897 Å) was used for the cobalt-containing matrices.

Transmission electron microscopy. TEM investigations were made using a Topcon 002B electron microscope operating at 200 kV with a point-to-point resolution r = 1.8 Å. The samples were sonicated in ethanol and deposited on a copper grid, which is covered with a holey carbon film.

Magnetic measurements. Isothermal magnetizations were measured using a Princeton Applied Research vibrating sample magnetometer Model 155 (VSM-maximum static field of ±1.8 T). High temperature susceptibility was measured using a Faraday balance equipped with an oven operating under controlled atmosphere (vacuum, air, argon, N_2 : H_2 = 95 : 5 or pure H_2) between 20 and 1000 °C and a field of up to 10 kOe.

Results and discussion

Characterization of the matrices

The mesoporous MCM-41 and xerogel matrices have been characterized before impregnation. The adsorption–desorption isotherms are shown in Fig. S-1 of the ESI‡ and the resulting parameters are summarized in Table 1. The xerogels appear to be of type E,[61] characteristic of a porosity constituted of aggregates of small spherical particles, while the MCM-41 matrix is of type A, characteristic of open tubular porosity.[61] We note the absence of microporosity in the MCM-41 matrix and only a negligible contribution (70 $m^2\ g^{-1}$) in the xerogels.

The absence of X-ray diffraction patterns for the xerogels indicates they are amorphous, whereas diffraction peaks observed at low angles (between 0.5 and 10°) for the MCM-41 matrix (Fig. 1) suggest some ordering. The four diffraction peaks correspond to a hexagonal array with a lattice parameter of 4.2 nm (walls plus pores). This structure is confirmed by TEM observations (Fig. 1b). According to the pore size mentioned previously, the wall size can be estimated to be 1.5 nm (Fig. 1c). In view of these characterizations, it is reasonable to consider these two matrices as similar except for their porosity arrangement. Consequently, this will allow

Table 1 Porosity parameters for both matrices

Matrix	Specific area/$m^2\ g^{-1}$	Porous volume/$cm^3\ g^{-1}$	Pores diameter/nm
Xerogels	896	0.926	2.0
MCM-41	1059	0.975	2.7

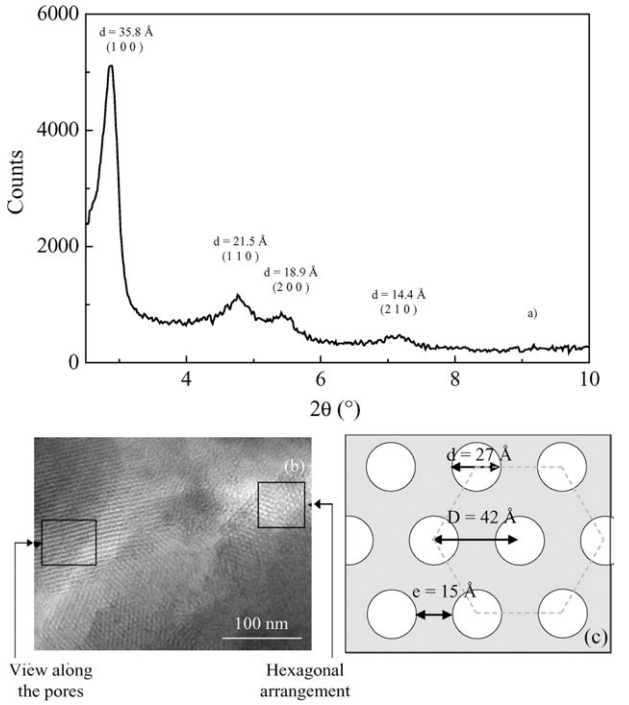

Fig. 1 Small angle XRD pattern (a), TEM micrography (b), and schematic representation of the porosity for MCM-41 (c).

us to study the effect of the porosity order on the spatial distribution of the nanoparticles formed.

From cluster to nanoparticles

To incorporate the cluster inside the matrices we have used an impregnation technique, well-known for the preparation of catalysts.[62–64] Several literature methods have been tested[65–74] and the most suitable for our cluster is that reported in ref. 67. Because of their dimensions, and to avoid concentration gradients, the monolithic xerogels were previously ground to a fine powder. Prior to impregnation, both matrices were dried at 100 °C under reduced pressure. After cooling, a saturated solution of the cluster (c = 0.39 mol L^{-1}) in THF was added in large excess and the resulting suspension was stirred for 24 h. The matrices were filtered and carefully rinsed several times with THF until a colourless filtrate was obtained, in order to remove the clusters deposited at their external surface and to ensure that the remaining clusters are only located inside their accessible porosity. After this crucial washing procedure, the matrices were dried at room temperature under vacuum overnight and finally stored under inert atmosphere. When diluted cluster solutions were used (*ca.* 10^{-3} mol L^{-1}), a partial discoloration of the solutions was observed, which suggests strong interactions between the cluster and the matrix (Fig. S-2 of the ESI‡). Energy Dispersive X-ray analysis (EDX) has shown that when saturated solutions of the clusters are used, Co : Si ratios of 2 and 5 wt% are reproducibly obtained for xerogels and MCM-41, respectively.

Since cobalt atoms in the precursor cluster are already in a low oxidation state, and the thermal activation of the cluster results in loss of CO, no additional reducing atmosphere

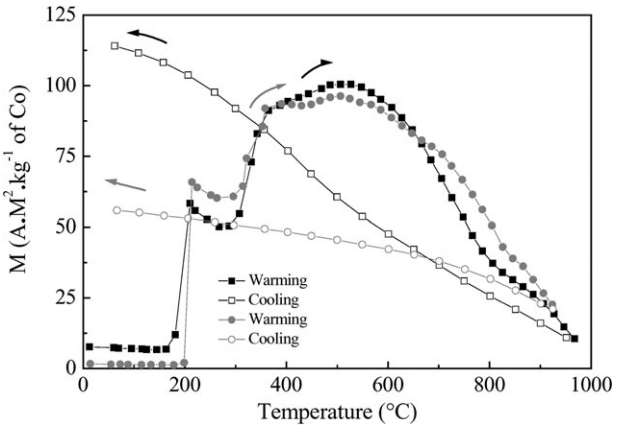

Fig. 2 Magnetic behaviour of the cluster incorporated in the matrices under argon (■,□: xerogel; ●,○: MCM-41) as a function of temperature.

should be necessary during the thermal treatments in order to obtain metallic nanoparticles. Thermogravimetric analyses under an argon atmosphere have shown that the pure, unsupported molecular cluster begins to degrade at 150 °C and is totally decomposed at 220 °C. However, once incorporated inside the matrices, it is significantly stabilized since the full degradation temperature is increased by more than 100 °C (340 °C for clusters in MCM-41 and 310 °C for clusters in xerogel). This confirms the existence of a strong cluster–matrix interaction. Magnetic studies (Fig. 2) indicate that cluster decomposition occurs at higher temperature in MCM-41 (200 °C) than in xerogel (180 °C), which is confirmed by infrared and TG analyses.

Ex situ infrared spectroscopy on the impregnated matrices calcined in the temperature range 30–600 °C have shown that cluster decomposition occurs *via* an unidentified intermediate species that is formed around 200 °C.

The thermal degradation of the cluster incorporated inside the matrices has been followed using a Faraday balance equipped with a home-made device allowing work under a controlled atmosphere and temperatures up to 1000 °C. The magnetic measurements have been carried out with an applied field fixed to 10 kOe, under an argon atmosphere and from room temperature to 1000 °C with a warming rate of 200 °C h^{-1}. It was originally hoped that the thermal decomposition of the cluster $NEt_4[Co_3Ru(CO)_{12}]$ would lead to the formation of highly dispersed Co_3Ru nanoparticles. Considering the cobalt–ruthenium phase diagram (Fig. S-3 of the ESI‡), this alloy has a Curie temperature of 370 °C[75] and a room temperature bulk saturation magnetization normalized to the cobalt amount of 64.5 $A.m^2$ (kg^{-1} Co). The magnetic behaviour as a function of temperature is reported in Fig. 2 for both matrices.

Discussion of the *in situ* magnetic behaviour

A large increase in magnetization was observed around 200 °C, which corresponds to the decomposition of the organometallic cluster and the formation of magnetic nanoparticles. Since pure $NEt_4[Co_3Ru(CO)_{12}]$ has an electron

count of 60 and is diamagnetic at room temperature, the small magnetic contribution observed around room temperature must originate from paramagnetic impurities.

Cluster decomposition results in a rapid increase of magnetization, which is consistent with the formation of ferromagnetic Co_3Ru nanoparticles. This sudden increase in magnetization should be followed by a maximum (or plateau) and a more or less rapid decrease as ferromagnetic order begins to compete with thermal agitation (we recall that the Curie temperature for Co_3Ru is T_c = 370 °C). However, we do not observe this behaviour. Instead, a first maximum is observed at 210 °C, followed by a decrease of the magnetic signal up to 290 °C after which the magnetization gradually increases again. Maximum magnetization is observed around 500 °C, far above the T_c of Co_3Ru, suggesting the formation of a different ferromagnetic phase. Above 500 °C, the signal decreases due to thermal effects and a kink is noted around 800 °C (see below). It is important to note that the warming and cooling curves for both matrices are not reversible. We shall come back to this point later.

In the following part of this paper, we will try to understand why our system behaves in this unexpected manner. First, in order to eliminate the hypothesis of a possible oxidation of the cluster due to the presence of traces of oxygen in argon, we have performed a similar experiment on an impregnated xerogel using a $N_2 : H_2$ = 95 : 5 atmosphere. The behaviour is absolutely comparable, and even more surprising is that the magnetization on cooling to room temperature is lower [36 A $m^2 \cdot (kg^{-1}$ Co)] than that of the sample treated under argon [116 A $m^2 \cdot (kg^{-1}$ Co)]. This unexpected behaviour appears to be intrinsic to the system.

Magnetic behaviour from room temperature to 300 °C

In order to understand the first magnetization increase around 200 °C, two freshly prepared samples were treated (under argon) *in situ* in the thermomagnetic balance up to a maximum of 200 and 270 °C, respectively, and then quenched to room temperature under argon to avoid subsequent transformation. For the sample treated at 200 °C, TEM results presented in Fig. 3a reveal the presence of nanoparticles with an average diameter of 3.1 ± 0.9 nm. The size distribution (Fig. 3b) is of log-normal type and its FWHM is *ca.* 1.8 nm. Electron diffraction (Fig. 3c) shows concentric rings corresponding to hexagonal close packed (*hcp*) cobalt. The lattice parameters calculated from the micrographs give a = 0.249(2) nm and c = 0.401(2) nm, in good agreement with the theoretical values (a = 0.25031(5) nm and c = 0.40605(8) nm).[76]

For the sample treated at 270 °C, the average diameter of the particles determined by TEM is 3.2 ± 1.1 nm and its FWHM of *ca.* 2.2 nm (Fig. 4a and 4b). Electron diffraction (Fig. 4c) shows concentric rings corresponding to face centred cubic (*fcc*) cobalt, in this case. The lattice parameter calculated from the pattern gives a = 0.356(3) nm, in good agreement with the theoretical value of a = 0.35447(2) nm.[77]

Therefore, an increase of the temperature from 200 to 270 °C results in a small increase in the size of the cobalt particles and in a phase transition for the cobalt nanoparticles from *hcp* to *fcc*. Similar phenomena have been observed for

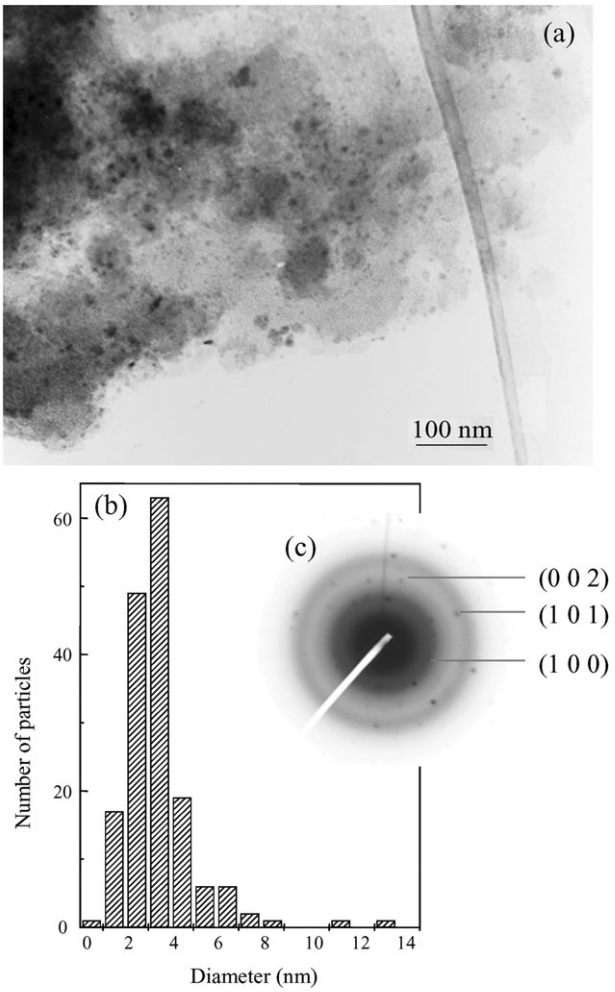

Fig. 3 TEM micrograph of the MCM-41 supported cluster material treated at 200 °C (a), size distribution of the nanoparticles (b) and electron diffraction pattern (c).

cobalt nanoparticles[78–79] and iron–cobalt alloy[80] nanoparticles. Although it is well-known that the hexagonal phase is thermodynamically more stable at low temperature, *fcc*-Co nanoparticles appear when their size exceeds 3.0 nm. Kitakami *et al.* associate this phase transition to a lower surface energy for *fcc*- compared to *hcp*-Co nanoparticles.[81]

The structural transition observed, from *hcp* to *fcc*, can be related to a change in the magnetocrystalline anisotropy constant. For a given temperature, the size of the particles (D_{S-F}), at which the system changes from unblocked to blocked magnetic state, is related to this anisotropy constant K. It has been found experimentally that even for *fcc*-Co, spherical nanocrystals present a dominating uniaxial anisotropy.[82,83] This critical size D_{S-F} is thus given by the following relation:[84]

$$D_{S-F} = \sqrt[3]{\frac{150 k_B T}{\pi K}}.$$

Concerning bulk magnetic materials, magnetostatic and magnetocrystalline energies are the main sources of anisotropy,[85] while for low-dimensional materials such as thin films,

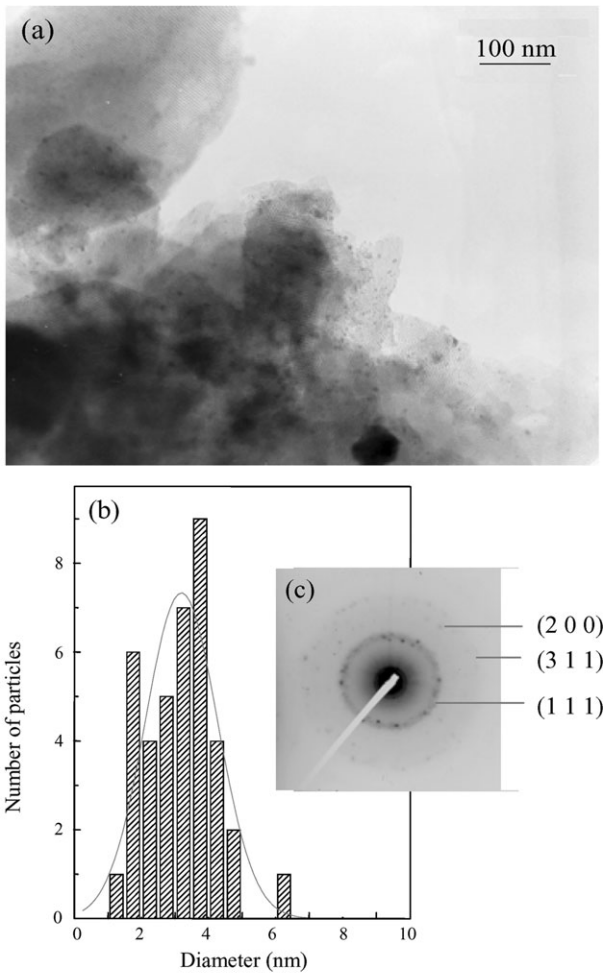

Fig. 4 TEM micrograph of the MCM-41 supported cluster material treated at 270 °C (a), size distribution of the nanoparticles (b) and electron diffraction pattern (c).

nanorods, nanowires or clusters, strong interfacial or surface effects are expected.[86–88] There is no single, well-defined K value for bulk cobalt in the literature and its value is experimentally known to depend on sample morphology, preparation, *etc*. For nanoparticles, it is also well-known that the anisotropy constant is increased with respect to the bulk value. Luis *et al*. have shown that the effective anisotropy constant decreases from 24×10^6 to 5×10^6 erg cm^{-3} when the size of the cobalt nanoparticles increases from 0.3 to 5 nm.[89–91] The net anisotropy of *fcc*- is smaller than that of *hcp*-bulk cobalt.[92] Considering the K values found in the literature, we report in Table 2 the estimated critical sizes D_{S-F} for both systems at different temperatures.

According to the particle size observed by TEM and reported in Table 2, the drop in magnetization observed in the 200–270 °C temperature range cannot be attributed to a change from an unblocked magnetic state to a blocked magnetic state. It is most likely that at 200 °C, and even at 270 °C, there is a mixture of *hcp*- and *fcc*-Co particles. If the balance is greatly in favor of *hcp*-Co at lower temperature (200 °C), it shifts to *fcc*-Co at higher temperature (270 °C). This phase

Table 2 Magnetic blocking critical sizes for cobalt at different temperatures

	K/erg cm^{-3}	D_{S-F}/nm at 20 °C	D_{S-F}/nm at 200 °C	D_{S-F}/nm at 270 °C
hcp-Co	4.1×10^6 (bulk)[93]	7.8	9.1	9.6
	13.0×10^6 (1.6 nm)[90]	5.3	6.2	6.5
fcc-Co	0.35×10^6 (bulk)[94]	17.6	20.7	21.7
	2.5×10^6 (bulk)[95–97]	8.9	10.5	11.0

transition induces a modification of the magnetization. The difficulty to observe saturation for superparamagnetic nanoparticles is well-documented.[32,85,98,99] Basic simulations of superparamagnetic behaviour using Langevin functions clearly show that for a given magnetic field, magnetization depends drastically on the size of the particles, temperature, *etc*. Considering the small increase of the average size of the particles compared to the change of anisotropy, and the fact that the critical size D_{S-F} is much higher in the case of *fcc*- than for *hcp*-Co, we can assign the observed drop in magnetization in the temperature range 200–290 °C to this phase transition.

Magnetic behaviour from 300 °C to 750 °C

We will now examine why the magnetic curves upon increasing and decreasing the temperature do not superimpose, that is to say, why the process is irreversible (Fig. 2). We have performed two *in situ* experiments under argon on impregnated MCM-41 with increasing temperature up to 500 and 700 °C, respectively. Once the system has reached this temperature, it was maintained for 13 h and 10 h, respectively, and finally cooled to room temperature. The results are reported in Fig. 5 and 6.

When the temperature is increased up to 500 °C, the magnetization increases and reaches its maximum. This behaviour is attributed to the increasing formation of metallic cobalt nanoparticles or to Ostwald ripening. Bazin *et al*.[100] have shown that reduction with pure di-hydrogen at 400 °C of a mixture of Ru and Co salts incorporated into NaY zeolite leads to the formation of separated metallic Co and Ru nanoparticles located in the cages of the matrix. When the temperature is decreased to room temperature after the 13 h plateau at 500 °C, the magnetization increased slightly to reach 115 A m^2 (kg^{-1} Co). This value does not correspond to pure cobalt, for which a value of 162 A m^2 (kg^{-1} Co) is expected, and therefore confirms Ru incorporation into cobalt-rich nanoparticles.[75] When the temperature is maintained at 500 °C, the magnetization first increases (insert of Fig. 5b) to reach a plateau and then decreases after 700 min. We have seen previously that the magnetic phase formed above 300 °C is either pure cobalt or a cobalt-rich phase but not the expected Co_3Ru alloy. Therefore, one can explain the decrease in magnetization by some (or more) ruthenium incorporation into the cobalt-rich nanoparticles. Indeed, it is well-known that increasing the ruthenium content in cobalt–ruthenium alloys decreases their Curie temperatures, and that above 30% of Ru, the particles are no longer ferromagnetic at room temperature.[75]

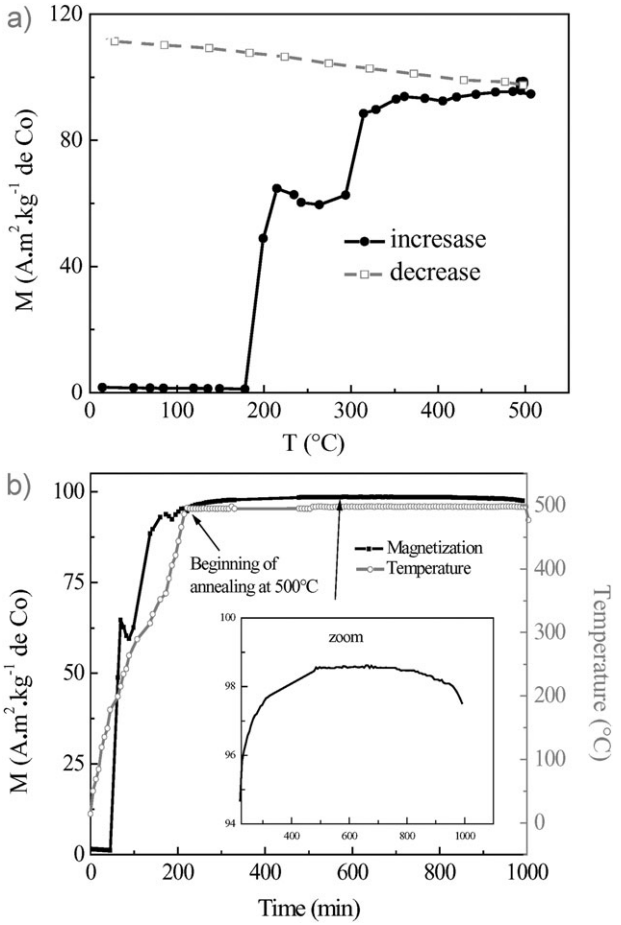

Fig. 5 Temperature (a) and time (b) dependence of the magnetization of a cluster-impregnated MCM-41 treated under argon, step: 13 h at 500 °C.

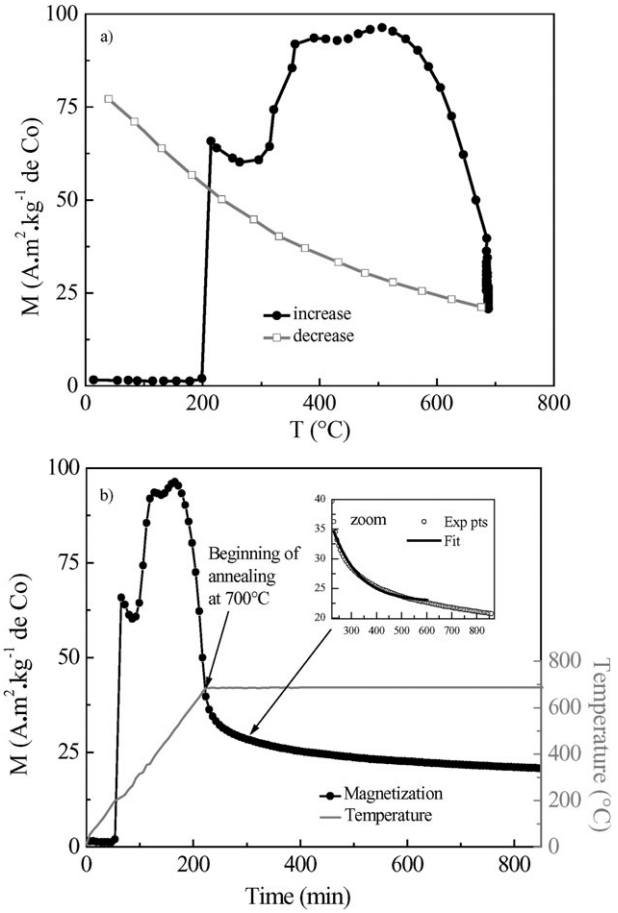

Fig. 6 Temperature (a) and time (b) dependence of the magnetization of a cluster-impregnated MCM-41 treated under argon, step: 10 h at 700 °C.

After the maximum magnetization has been reached around 500 °C, a decrease is observed with increasing temperature (Fig. 6a) owing to thermal agitation. When the temperature is maintained at 700 °C (Fig. 6) for 10 h, an exponential decrease of the magnetization is observed which reaches *ca.* 20 A m^2 (kg^{-1} Co) (Fig. 6b). The saturation magnetization obtained after cooling to room temperature is 83 A m^2 (kg^{-1} Co), far below the bulk metallic cobalt value [161 A m^2 (kg^{-1} Co)] and higher than that for Co_3Ru [64.5 A m^2 (kg^{-1} Co)]. All these observations confirm a compositional change of the metallic alloy as a function of temperature.

At this stage, one can formulate the hypothesis that when the organometallic cluster decomposes, cobalt and ruthenium would segregate and form cobalt (pure) and ruthenium (pure or alloyed with small amounts of cobalt) metallic nanoparticles. Increasing temperatures result in the reorganisation of the system and to alloy formation and therefore to a decrease of the magnetization.

The nature and structure of the phases formed during these two treatments have been investigated by TEM and XRD. After treatment at 500 °C, electron diffraction on an assembly of nanoparticles showed (Fig. 7) that they have a *fcc* structure with a lattice parameter of 0.354(2) nm, close to the theoretical value (0.35447 nm). The size distribution looks like a log-normal distribution for which the maximum is situated at 5.1 nm and with FWHM of 8.5 nm.

When the sample was treated at 700 °C, the particles observed were larger than those obtained at 500 °C. The shape of the distribution can be simulated with a log-normal function centred at 6.7 nm and with FWHM of 11.3 nm (Fig. 8). A few, much larger particles (120 nm) were observed in the vicinity of these small particles. Electron diffraction patterns obtained from an assembly of small particles are similar to those obtained for the sample treated at 500 °C and confirm the presence of *fcc* particles. Electron diffraction measurements (Fig. 8b) have been performed on individual particles with a size larger than 10 nm and reveal the presence of a hexagonal phase. The lattice parameters calculated are reported in Table 3 and are intermediate between those for the $P6_3/mmc$ hexagonal phases of pure cobalt[75] and ruthenium.[101]

EDX analysis on these large particles confirms the presence of ruthenium and diffraction simulations with CaRIne software[102] (Fig. 8b) considering a hexagonal structure (space group: $P6_3/mmc$) with lattice parameters $a = 0.258(3)$ and $c = 0.411(2)$ nm fit well the experimental patterns. Because TEM gives a local view of the materials, we have used XRD diffraction to gain a more global view of our two samples, as this technique is more sensitive to the larger particles. The

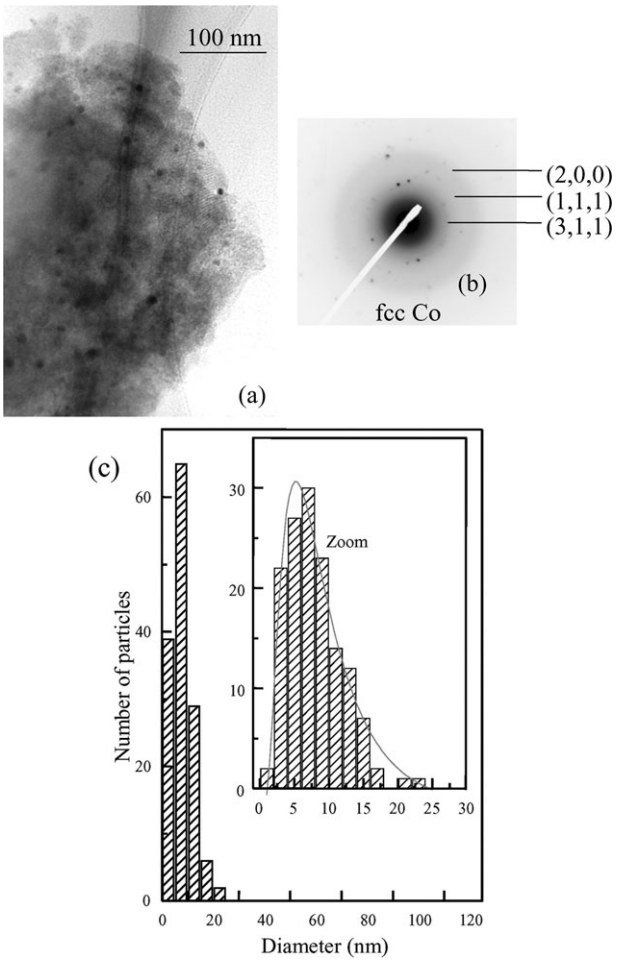

Fig. 7 TEM micrograph of the cluster-impregnated MCM-41 treated at 500 °C (a), electron diffraction pattern (b), and size distribution of the nanoparticles (c).

XRD pattern obtained with the sample treated at 700 °C (Fig. 9b) is rather similar to that obtained for bulk Co_3Ru alloy (Fig. 9c), thus confirming its formation after 10 h of treatment at this temperature.

For the sample treated at 500 °C for 10 h (Fig. 9a), two phases were evidenced. The first one corresponds to a *fcc* phase, probably the cobalt phase observed by TEM. Since these particles are quite small, the intensity of the diffraction lines remains weak. The second phase has diffraction lines similar to the Co_3Ru alloy with positions appearing at smaller diffraction angles. The lattice parameters of the different phases observed have been calculated and are reported in Table 4 and in Fig. 10.

For the samples treated at 500 °C, besides the *fcc*-Co phase observed by TEM for the smaller particles, a second phase has been detected using XRD, which is a Co–Ru alloy containing $57 \pm 8\%$ of Ru. According to the magnetic phase diagram it is paramagnetic, and this is probably why it was not observed by *in situ* magnetic measurements. When the system is heated up to 700 °C, the particles obtained tend toward the nominal composition of the cluster (*i.e.* Co_3Ru).

We have shown with the Ru–Co system that bimetallic nanoparticles can be obtained by thermal treatment of heterometallic clusters incorporated in mesoporous silica matrices under an inert atmosphere. It should be mentioned that Zitoun *et al.*[103–104] have prepared narrow size-distributed bimetallic Co_xRu_y nanoparticles by decomposition under mild conditions (room temperature and under 3 bars of dihydrogen) of a mixture of organometallic precursors in a polymer (polyvinylpyrrolidone).

Magnetic behaviour from 750 to 1000 °C and back to room temperature

When the treatment temperature is further increased above 750 °C, a kink is observed on the magnetic curve (Fig. 2). This can be attributed to the presence of two magnetic phases with different Curie temperatures. Extrapolation of the two parts of the curves (before and after the kink) to the *x*-axis allows us to estimate their Curie temperatures. Both values obtained ($T_{c_1} \approx 850$ °C and $T_{c_2} \approx 1100$ °C) confirm the presence of magnetic phases with a composition different from that of the cluster. According to the phase diagram (Fig. S-3 of the ESI‡), the first magnetic phase with $T_{c_1} = 850$ °C can be associated to a Co–Ru alloy containing 7% Ru (in the case of *fcc* alloy) or 12% Ru (in the case of *hcp*- alloy). The second phase ($T_{c_2} = 1100$ °C) is associated with pure cobalt nanoparticles.

Finally, when returning to room temperature, we note that the warming and cooling curves for both matrices do not superimpose. More surprising is that the magnitude of the magnetization is lower on cooling than on warming. A ripening or annealing of the particles formed would lead to an opposite behaviour. This suggests that the phase(s) formed during *in situ* decomposition below 800 °C is (are) not at thermodynamic equilibrium.

Discussion of the *ex situ* magnetic behaviour

Ex situ treatments at 250, 500, 700 and 900 °C for 1 h, 5 h and 10 h have been performed on the impregnated cluster in both types of host. Due to the small size of the particles formed, no diffraction lines were observed on the XRD patterns of the samples treated at 250 °C and only weak lines in those treated at 500 °C. From the XRD study on the samples treated at 500 °C (for longer periods) and above, some conclusions can be drawn, although they are only applicable to the larger particles, which are consistent with the observations made in the *in situ* study. The major phase present at low temperature (but above 300 °C) and short treatment times is *fcc*-Co, but this phase disappears progressively to form *hcp*-Co–Ru alloy and the composition tends to the (Co_3Ru) cluster nominal composition (Fig. 11) for higher temperatures and longer treatment times.

TEM studies show that the particles formed are spatially better distributed in MCM-41 than in xerogels. This is in good agreement with what we would expect comparing an amorphous structure (xerogel) with a well ordered one (MCM-41).

Whatever the matrix, two populations of particles were observed. On the one hand, very small particles (average size: 1.8 nm in MCM-41 and between 2.2 and 2.9 in xerogels) with a narrow size distribution that remain unchanged upon increasing the temperature. Considering the pore characteristics of these two matrices (2.7 and 2.0 nm diameter for MCM-41 and

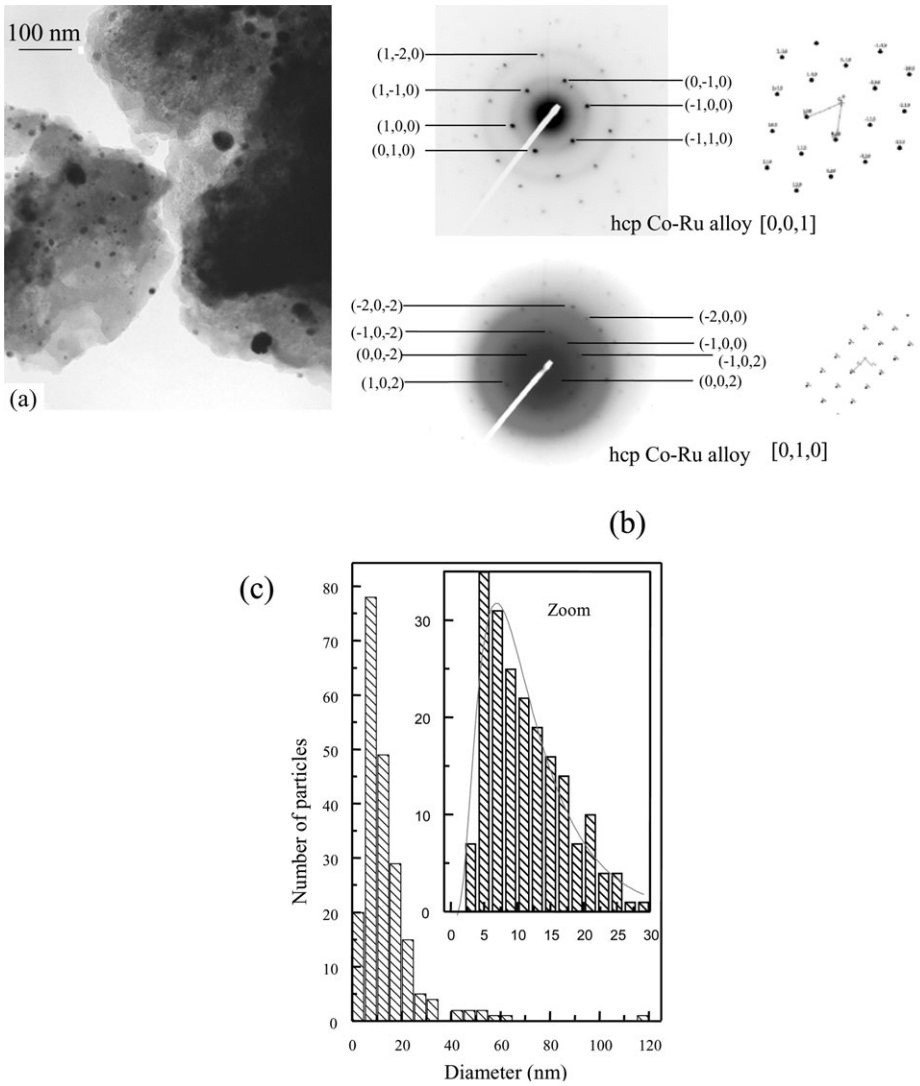

Fig. 8 TEM micrograph of the cluster-impregnated MCM-41 treated at 700 °C (a), electron diffraction patterns (b) and size distribution of the nanoparticles (c).

xerogels, respectively), it seems that these ''native'' particles are constrained by the matrix porosity. Due to the 3D-disordered structure of the xerogels, the size distribution of their pores is broader than for the MCM-41, leading to larger particles. These small particles are either pure cobalt or pure ruthenium. On the other hand, when the temperature increases, some of the particles at the vicinity of the surface of the material break the silica network and grow at the expense of the ''native'' particles, forming Co–Ru alloys. A similar phenomenon has already been observed by Schünemann

Table 3 Theoretical lattice parameters of pure cobalt and ruthenium and experimental values for our MCM-41 sample treated at 700 °C for 10 h

	Co/nm	Ru/nm	Observed Parameter/nm
a	0.25031(5)	0.27058(1)	0.258(3)
c	0.40605(8)	0.42811(2)	0.411(2)

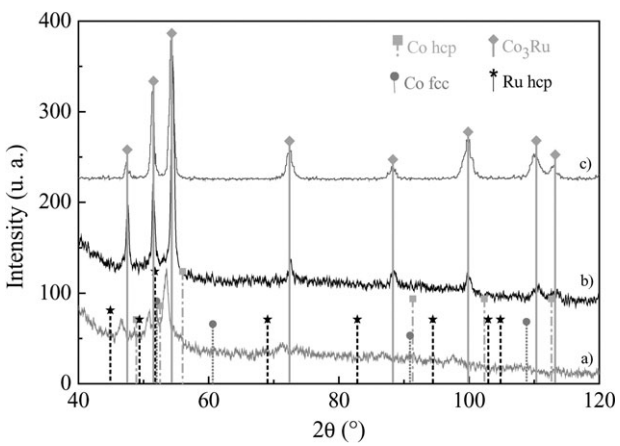

Fig. 9 XRD pattern of the cluster-impregnated MCM-41 treated at 500 °C (a) and 700 °C (b) during 10 h and, for comparison, of a bulk Co_3Ru alloy.

Table 4 Theoretical and calculated lattice parameters from XRD pattern (Fig. 9) and TEM electronic diffraction (Fig. 8b)

	Theoretical *hcp*-Co	Theoretical *hcp*-Ru	Bulk Co_3Ru alloy	After 10 h at 700 °C		After 10 h at 500 °C
				By XRD	By TEM	By XRD
a/nm	0.25031(5)	0.27058(1)	0.2567(2)	0.2553(7)	0.258(3)	0.2620(9)
c/nm	0.40605(8)	0.42811(2)	0.4119(4)	0.4098(8)	0.411(2)	0.4199(7)

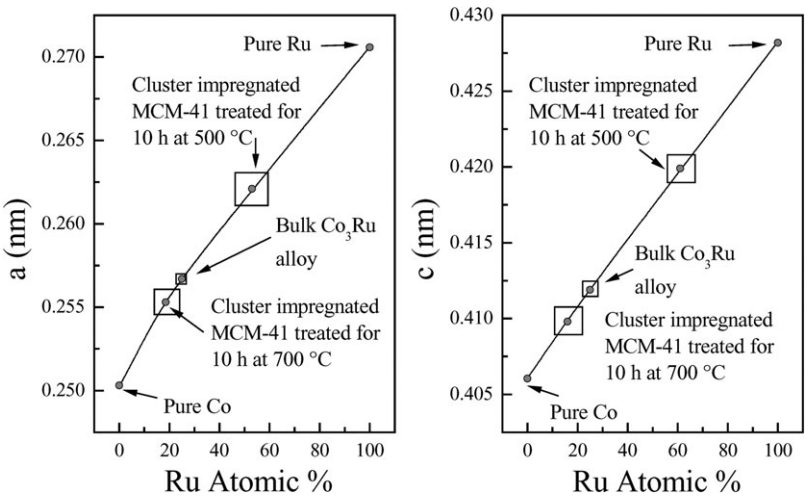

Fig. 10 Theoretical lattice parameters *a* and *c* as a function of the ruthenium content in Co–Ru alloys and calculated for our samples treated, respectively at 500 and 700 °C.

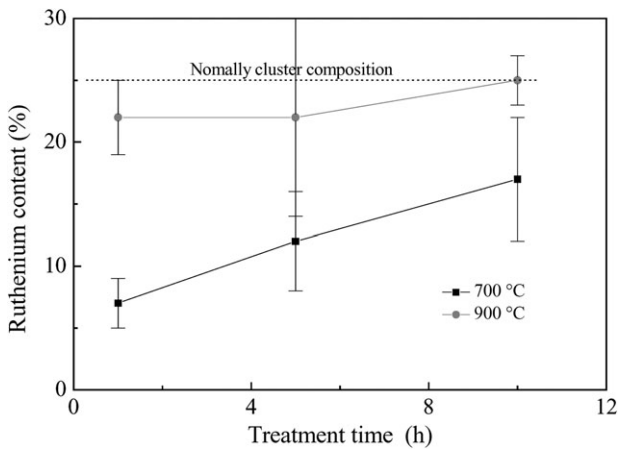

Fig. 11 Evolution of ruthenium content as a function of the thermal treatment.

et al.[105] for metallic iron nanoparticles formed by decomposition of iron pentacarbonyl in NaX zeolite. These authors obtained two populations of particles, small ones (1.2 nm diameter) in the cages of the matrix and larger ones (3.0 mm) located at structural defects on the zeolite.

Isothermal magnetization measurements have been performed at room temperature on these series of samples. It is difficult to extract any quantitative information as the system is different at each temperature, matrix, and duration of thermal treatments. However, we observe ferromagnetic behaviour without saturation at low treatment temperatures, such as 250 °C, and when saturation magnetization is observed it goes through a maximum around 500 °C. This confirms the presence of size-distributed superparamagnetic or ferromagnetic nanoparticles, the nature of which changes with the duration and temperature of the thermal treatment.

Conclusions

By using *in situ* and *ex situ* techniques, it has been possible to partially elucidate the formation of the intermetallics (Co–Ru) through the decomposition of the well-defined bimetallic molecular cluster $NEt_4[CoRu_3(CO)_{12}]$ confined in mesoporous silica matrices. At 200 °C, the cluster decomposes *via* an unidentified intermediate into segregated metallic nanoparticles of *hcp*-Ru and *hcp*-Co. The latter is transformed to *fcc*-Co above 270 °C. On further heating, alloying occurs between Ru and Co and the percentage of Ru increases progressively to the final stoichiometry of the starting cluster, $CoRu_3$. Whether the alloying occurs at the surface or the core remains unknown. For practical application, the ordered mesoporous silica (MCM-41) appears to be more suitable for obtaining a narrower and even distribution of size of nanoparticles.

Acknowledgements

We acknowledge support from the Ministère de la Recherche, the Centre National de la Recherche Scientifique, and the Région Alsace (doctoral grant to F.S.). C.E. would like to thank Dr M. Kurmoo for fruitful discussions.

References

1 G. Schmid, *Chem. Rev.*, 1992, **92**, 1709.

2 *Clusters and Colloids: From Theory to Applications*, ed. G. Schmid, John Wiley & Sons, New York, 1994.
3 C. R. Martin, *Science*, 1994, **266**, 1961.
4 A. P. Alivisatos, *Science*, 1996, **271**, 933.
5 J. Shi, S. Gider, D. Babcock and D. D. Awschalom, *Science*, 1996, **271**, 937.
6 D. Rouvray, *Chem. Ber*., 2000, **36**, 46.
7 G. Lawton, *Chem. Ind*., 2001, 174.
8 K. Havancsak, *Mater. Sci. Forum*, 2003, **414–415**, 85.
9 *Nanostructures and Quantum Effects*, ed. H. Sakaki and H. Noge, Springer-Verlag, Berlin, 1994.
10 *Optical Properties of Semiconductor Quantum Dots*, ed. U. Woggon, Springer-Verlag, Berlin, 1997.
11 *Nanomagnetism*, ed. A. Hernando, Kluwer Academic Publishers, Dordrecht, The Netherlands, 1993.
12 *Magnetic Properties of Fine Particles*, ed. J. L. Dorman and D. Fiorani, North-Holland, Amsterdam, 1992.
13 *Science and Technology of Nanostructured Magnetic Materials*, ed. George C. Hadjipanayis and G. Prinz, Plenum Press, New York, 1991.
14 B. F. G. Johnson, *Top. Catal*., 2003, **24**, 1–4, 147.
15 *Metal Clusters in Chemistry*, ed. P. Braunstein, L. A. Oro and P. R. Raithby, Wiley-VCH, Weinheim, 1999, vol. 2.
16 B. L. Cushing, V. L. Kolesnichenko and C. J. O'Connor, *Chem. Rev*., 2004, **104**, 3893, and references therein.
17 *Encyclopedia of Nanoscience and Nanotechnology*, ed. Nalwa Hari Singh, American Scientific Publishers, 2004, vol. 1, p. 687.
18 I. M. L. Billas, A. Chatelain and W. A. de Heer, *Science*, 1994, **265**, 1662.
19 A. J. Cox, J. G. Louderback, S. E. Apsel and L. A. Bloomfield, *Phys. Rev. B*, 1994, **49**, 12295.
20 P. Villasenor-Gonzalez, J. Dorantes-Davila, H. Dreyssé and G. M. Pastor, *Phys. Rev. B*, 1997, **55**, 15084.
21 C. D'Orléans, J. P. Stoquert, C. Estournès, C. Cerruti, J. J. Grob, J. Guille, F. Haas, D. Muller and M. Richard-Plouet, *Phys. Rev. B*, 2003, **67**, 220101.
22 C. D'Orléans, J. P. Stoquert, C. Estournès, J. J. Grob, D. Muller, J. L. Guille, M. Richard-Plouet, C. Cerruti and F. Haas, *Nucl. Instrum. Methods Phys. Res., Sect. B*, 2004, **216**, 372.
23 C. Pham-Huu, N. Keller, C. Estournès, G. Ehret and M. J. Ledoux, *Phys. Chem. Chem. Phys*., 2003, **5**, 3716.
24 N. Cordente, C. Amiens, B. Chaudret, M. Respaud, F. Senocq and M.-J. Casanove, *J. Appl. Phys*., 2003, **94**, 10–6358.
25 O. Margeat, C. Amiens, B. Chaudret, P. Lecante and R. E. Benfield, *Chem. Mater*., 2005, **17**, 1–107.
26 J. Osuna, D. Caro, C. Amiens, B. Chaudret, E. Snoeck, M. Respaud, J.-M. Broto and A. Fert, *J. Phys. Chem*., 1996, **100**, 14571.
27 M. Respaud, J.-M. Broto, H. Rakoto, A. R. Fert, L. Thomas, B. Barbara, M. Verelst, E. Snoeck, P. Lecante, A. Mosset, J. Osuna, T. O. Ely, C. Amiens and B. Chaudret, *Phys. Rev. B*, 1998, **57**, 2925.
28 T. Ould Ely, C. Amiens, B. Chaudret, E. Snoeck, M. Verelst, M. Respaud and J.-M. Broto, *Chem. Mater*., 1999, **11**, 526.
29 T. Ould Ely, C. Pan, C. Amiens, B. Chaudret, F. Dassenoy, P. Lecante, M.-J. Casanove, A. Mosset, M. Respaud and J.-M. Broto, *J. Phys. Chem. B*, 2000, **104**, 695.
30 C. Estournès, N. Cornu and J. L. Guille, *J. Non-Cryst. Solids*, 1994, **170**, 287.
31 C. Estournès, T. Lutz and J. L. Guille, *J. Non-Cryst. Solids*, 1996, **197**, 192.
32 C. Estournès, T. Lutz, J. Happich, T. Quaranta, P. Wissler and J. L. Guille, *J. Magn. Magn. Mater*., 1997, **173**, 83.
33 T. Lutz, C. Estournès, J. C. Merle and J. L. Guille, *J. Alloys Compd*., 1997, **262–263**, 438.
34 O. Cíntora-González, D. Muller, C. Estournès, M. Richard-Plouet, R. Poinsot, J. J. Grob and J. Guille, *Nucl. Instrum. Methods Phys. Res., Sect. B*, 2001, **178**, 144.
35 C. D'Orléans, J. P. Stoquert, C. Estournès, C. Cerruti, J. J. Grob, J. Guille, F. Haas, D. Muller and M. Richard-Plouet, *Nucl. Instrum. Methods Phys. Res., Sect. B*, 2003, **209**, 316.
36 M. Chatterjee, T. Iwasaki, Y. Onodera and T. Nagase, *Catal. Lett*., 1999, **61**, 199.
37 Y.-J. Han, J. M. Kim and G. D. Stucky, *Chem. Mater*., 2000, **12**, 2068.
38 Z. Liu, Y. Sakamoto, T. Ohsuna, K. Hiraga, O. Terasaki, C. H. Ko, H. J. Shin and R. Ryoo, *Angew. Chem., Int. Ed*., 2000, **39**, 3107.
39 A. Fukuoka, N. Higashimoto, Y. Sakamoto, M. Sasaki, N. Sugimoto, S. Inagaki, Y. Fukushima and M. Ichikawa, *Catal. Today*, 2001, **66**, 23.
40 A. Fukuoka, N. Higashimoto, Y. Sakamoto, S. Inagaki, Y. Fukushima and M. Ichikawa, *Microporous Mesoporous Mater*., 2001, **48**, 171.
41 S. Hermans, R. Raja, J. M. Thomas, B. F. G. Johnson, G. Sankar and D. Gleeson, *Angew. Chem., Int. Ed*., 2001, **40**, 1211.
42 M. Jones, M. Duer, S. Hermans, Y. Khimyak, B. Johnson and J. Thomas, *Angew. Chem., Int. Ed*., 2002, **41**, 4726.
43 H. R. Chen, J. L. Shi, Y. S. Li, J. N. Yan, Z. L. Hua, H. G. Chen and D. S. Yan, *Adv. Mater*., 2003, **15**, 1078.
44 S. Hermans, S. Sadasivan, C. M. G. Judkins, B. F. G. Johnson, S. Mann and D. Khushalari, *Adv. Mater*., 2003, **15**, 1853.
45 P. Braunstein, H.-P. Kormann, W. Meyer-Zaika, R. Pugin and G. Schmid, *Chem.–Eur. J*., 2000, **6**, 4637.
46 J. S. Jung, K. H. Choi, Y. K. Jung, S. H. Lee, V. O. Golub, L. Malkinski and C. J. O'Connor, *J. Magn. Magn. Mater*., 2004, **272–276**, 1157.
47 P. Wu, J. Zhu and Z. Xu, *Adv. Funct. Mater*., 2004, **14**, 4–345.
48 T. A. Crowley, K. J. Ziegler, D. M. Lyons, Do. Erts, H. Olin, M. A. Morris and J. D. Holmes, *Chem. Mater*., 2003, **15**, 18–3518.
49 R. Köhn, D. Paneva, M. Dimitrov, T. Tsoncheva, I. Mitov, C. Minchev and M. Fröba, *Microporous Mesoporous Mater*., 2003, **63**, 125.
50 A. A. Eliseev, K. S. Napolskii, A. V. Lukashin and Y. D. Tretyakov, *J. Magn. Magn. Mater*., 2004, **272–276**, 1609.
51 F. Schweyer-Tihay, P. Braunstein, C. Estournès, J. L. Guille, B. Lebeau, J. L. Paillaud, M. Richard-Plouet and J. Rosé, *Chem. Mater*., 2003, **15**, 57.
52 X. G. Zhao, J. L. Shi, B. Hu, L. X. Zhang and Z. L. Hua, *J. Mater. Chem*., 2003, **13**, 399.
53 S. L. Brock, S. C. Perera and K. L. Stamm, *Chem.–Eur. J*., 2004, **10**, 3364.
54 P. Braunstein and J. Rosé, *Heterometallic Clusters for Heterogeneous Catalysis*, in *Catalysis by Di- and Polynuclear Metal Clusters*, ed. R. D. Adams and F. Cotton, John Wiley, New-York, 1998, pp. 443–508.
55 P. Braunstein, R. Bender and J. Kervennal, *Organometallics*, 1982, **1**, 1236.
56 (*a*) P. Braunstein, J. Kervennal and J.-L. Richert, *Angew. Chem., Int. Ed. Engl*., 1985, **24**, 768; (*b*) P. Braunstein, J. Kervennal and J.-L. Richert, *Angew. Chem., Int. Ed. Engl*., 1985, **97**, 762.
57 F. Schweyer, P. Braunstein, C. Estournès, J. Guille, H. Kessler, J.-L. Paillaud and J. Rosé, *Chem. Commun*., 2000, 1271.
58 A. C. Voegtlin, A. Matijasic, J. Patarin, C. Saulerand, Y. Grillet and L. Hure, *Microporous Mater*., 1997, **10**, 137.
59 N. Viart and J.-L. Rehspringer, *J. Non-Cryst. Solids*, 1996, **195**, 223.
60 P. Braunstein and J. Rosé, *Inorg. Synth*., 1989, **26**, 356.
61 J. H. De Boer, in *The Structure and Properties of Porous Materials*, ed. D. H. Everett and F. S. Stone, Butterworths, London, 1958.
62 R. L. Augustine, *Heterogeneous Catalysis for the Synthetic Chemist*, Marcel Dekker, New York, 1996, ch. 13.
63 J. A. Schwartz, *Chem. Rev*., 1995, **95**, 447.
64 P. Braunstein and J. Rosé, in *Metal Clusters in Chemistry*, ed. P. Braunstein, L. A. Oro and P. R. Raithby, Wiley-VCH, Weinheim, 1999, vol. 2, p. 616.
65 E. Van Steen, G. S. Sewell, R. A. Makhothe, C. Micklewaite, H. Manstein, M. de Lange and C. T. O'Connor, *J. Catal*., 1996, **162**, 220.
66 B. Heinrichs, F. Noville and J.-P. Pirard, *J. Catal*., 1997, **170**, 366.
67 M. Che, O. Clause and C. Marcilly, in *Preparation of Solid Catalysts*, ed. G. Ertl, H. Knoezinger and J. Weitkamp, Paris, 1999, p. 315.
68 A. Dandekar, R. T. K. Baker and M. A. Vannice, *J. Catal*., 1999, **183**, 131.
69 H. Kraus and R. Prins, *J. Catal*., 1996, **164**, 251.
70 J. De Graff, A. J. Van Dillen, K. P. De Jong and D. C. Koningsberger, *J. Catal*., 2001, **203**, 307.

71 T. Bécue, R. J. Davis and J. M. Garces, *J. Catal*., 1998, **179**, 129.
72 M. Reinikainen, M. K. Nimelä, N. Kakuta and S. Suhonen, *Appl. Catal., A*, 1998, **174**, 61.
73 Y. Huang, X. Meng, Z. Dang, S. Weng and C. J. Zhang, *J. Chem. Soc., Chem. Commun*., 1995, 1025.
74 M. Reinikainen, J. Kiviaho, M. Kröger, M. K. Nimelä and S. Jääskeläinen, *J. Mol. Catal. A: Chem*., 1997, **118**, 137.
75 Landolt-Börnstein, Zahlenwerte und Funktionen, 9. Teil, Magnetic Properties I, Springer Verlag, Berlin, 1961.
76 JCPDS file no 05-0727, International Center for Diffraction Data.
77 JCPDS file no 15-0806, International Center for Diffraction Data.
78 R. H. Kodama, *J. Magn. Magn. Mater*., 1999, **200**, 359.
79 A. Muller-Gattang, C. Estournès, T. Lutz, M. Richard-Plouet and J. L. Guille, *J. Non-Cryst. Solids,* to be published.
80 Y. I. Petrov and E. A. Shafranovsky, *J. Nanopart. Res*., 2001, **3**, 419.
81 O. Kitakami, H. Sato, Y. Shimada, F. Sato and M. Tanaka, *Phys. Rev. B*, 1997, **56**, 21–13849.
82 M. Jamet, W. Wernsdorfer, C. Thirion, D. Mailly, V. Dupuis, P. Mélinon and A. Pérez, *Phys. Rev. Lett*., 2001, **86**, 4676.
83 W. Wernsdorfer, C. Thirion, N. Demoncy, H. Pascard and D. Mailly, *J. Magn. Magn. Mater*., 2002, **242–245**, 132.
84 C. P. Bean and I. S. Jacobs, *Appl. Phys*., 1953, **25**, 302.
85 A. Herpin, *Théorie du Magnétisme*, PUF, Paris, France, 1968.
86 J. L. Dormann, D. Fiorani and E. Tronc, in *Advances in Chemical Physics*, ed. I. Prigogine and Stuart A. Rice, Wiley, New York, 1997, vol. XCVIII.
87 N. Nakajima, T. Koide, T. Shidara, H. Miyauchi, H. Fukutani, A. Fujimori, K Iio, T. Katayama, M. Nývlt and Y. Suzuki, *Phys. Rev. Lett*., 1998, **81**, 5229.
88 J. Dorantes-Davila and G. M. Pastor, *Phys. Rev. Lett*., 1998, **81**, 208.
89 F. Luis, J. M. Torres, L. M. García, J. Bartolomé, J. Stankiewicz, F. Petroff, F. Fettar, J.-L. Maurice and A. Vaurès, *Phys. Rev. B*, 2002, **65**, 094409.
90 Y. Xie and J. A. Blackman, *J. Phys.: Condens. Matter*, 2004, **16**, 3163.
91 M. Respaud, *J. Appl. Phys*., 1999, **86**, 1–556.
92 G. A. Held, G. Grinstein, H. Doyle, S. Sun and C. B. Murray, *Phys. Rev. B*, 2001, **64**, 2408.
93 C. Kittel, in *Introduction to Solid State Physics*, 7th ed., John Wiley & Sons, Inc., New York, 1996.
94 W. Gong, H. Li, Z. Zhao and J. Chen, *J. Appl. Phys*., 1991, **69**, 8–5119.
95 J. P. Chen, C. M. Sorensen, K. J. Klabunde and G. C. Hadjipanayis, *J. Appl. Phys*., 1994, **76**, 6316.
96 W. D. Doyle and P. J. Flanders, in *International Conference of Magnetism, Nottingham, 1964*, The Institute of Physics and the Physical Society, Bristol, 1965, p. 751.
97 W. A. Sucksmith and J. E. Thompson, *Proc. R. Soc. London, Ser. A*, 1954, **225**, 362.
98 J. L. Dormann, D. Fiorani and E. Tronc, in *Advances in Chemical Physics*, ed. I. Prigogine and S. A. Rice, John Wiley and Sons Inc., New York, 1997, vol. 18.
99 I. S. Jacobs, C. P. Bean, in *Magnetism t. III*, ed. G.T. Rado and H. Suhl, Academic Press, New York, 1963, **271**, p. 8.
100 D. Bazin, I. Kovács, J. Lynch and L. Guczi, *Appl. Catal., A*, 2003, **242**, 179.
101 JCPDS file no. 06-0663, International Center for Diffraction Data.
102 CaRIne Crystallography software.
103 D. Zitoun, M. Respaud, M.-C. Fromen, P. Lecante, M.-J. Casanove, C. Amiens and B. Chaudret, *J. Magn. Magn. Mater*., 2004, **272–276**, 1536.
104 D. Zitoun, C. Amiens, B. Chaudret, M. C. Fromen, P. Lecante, M. J. Casanove and M. Respaud, *J. Phys. Chem. B*, 2003, **107**, 6997.
105 V. Schünemann, H. Winkler, C. Butzlaff and A. X. Trautwein, *Hyperfine Interact*., 1994, **93**, 1427.